Organic Electronics 32 (2016) 59–64

Contents lists available at ScienceDirect

Organic Electronics

journal homepage: www.elsevier.com/locate/orgel

Multifunctional π-conjugated poly (3-methylthiophene) nanotubes for optoelectronic and field emissive devices

Young Ki Hong [a, 1], Seokho Kim [b, 1], Hyeong Tae Kim [b], Sunkook Kim [a], Bong-Gi Kim [c], Sunjong Lee [d, ***], Dong Hyuk Park [b, **], Bo-Hyun Kim [e, *]

[a] Department of Electronics and Radio Engineering, Kyung Hee University, Gyeonggi 446-701, South Korea
[b] Department of Applied Organic Materials Engineering, Inha University, Incheon 402-751, South Korea
[c] Department of Organic and Nano System Engineering, Konkuk University, Seoul 143-701, South Korea
[d] Korea Institute of Industrial Technology, Chungcheongnam 31056, South Korea
[e] Department of Materials Science and Engineering, Korea Advanced Institute of Science and Technology, Daejeon 305-701, South Korea

ARTICLE INFO

Article history:
Received 26 January 2016
Received in revised form
6 February 2016
Accepted 11 February 2016
Available online 18 February 2016

Keywords:
Multifunctionality
Poly (3-methylthiophene)
Nanotube
Photoluminescence
Photocurrent
Field emission

ABSTRACT

Multifunctional properties of nanomaterials becomes a hot topic in nano research for the development of multifunctional devices, because modern devices need multifunctional platform for the high efficient plural performance on a single device. Here, we introduce a multifunctional π-conjugated poly (3-methylthiophene) (P3MT) nanotube (NT), showing controllable optical and electrical properties through the control of doping level. P3MT NTs were electrochemically synthesized in the low temperature (−40 °C) on the nanoporous template. The change of doping level by post cyclic voltammetry (CV) treatment on the P3MT lead the variance of polaron/bipolaron band, resulting into the drastic change of ultraviolet-visible absorption and photoluminescence properties. While P3MT NTs before CV treatment show an ohmic behavior in the current-voltage characteristics, those after CV treatment show high photocurrent. From the field emission experiment, the P3MT NTs before CV treatment have a relatively low turn-on electric field and stable electron emission property compared to the P3MT NTs after CV treatment. This shows that the π-conjugated polymers should be shed new light on their multifunctionality for the potential application to the multifunctional platform of opto-electronic nanodevices.

1. Introduction

Novel properties of nanomaterials have been enthusiastically pursued for decades due to the new needs for flexible and wearable sensors and opto-electronics. However, as the size of materials goes down into the nanoscale, the electrical, optical and physical properties of nanomaterials need to be studied again due to the quantum size effect causing different behaviors from their bulk properties [1,2]. Therefore, although the remarkable progresses have been reported [3–5], it still remains a challenging task to realize the nanoscale multifunctional devices using combination of monofunctional materials. For example, carbon nanotubes and inorganic semiconducting nanowires have shown the multifunctional properties applicable for the light emitters, photodetectors, field emitters and field effect transistors (FET) [6–8]. However, their delicate and non-reproducible fabrication process and complex of property control have drawn back the commercial devices. From decades ago, π-conjugated organic molecules and polymers have been popular because of their controllable electrical and optical properties as well as their relative easy synthetic process [9–12]. This provides versatile applications of π-conjugated materials such as organic light-emitting diode, organic thin-film transistor, organic photovoltaic cell, chemical/bio sensor, electrochromic device, and field emission display (FED) [13–18]. In addition, FETs fabricated by π-conjugated materials was reported to have the light-emitting natures [19–21]. Accordingly, nano-engineered π-conjugated polymers are worthy enough to be considered as a multifunctional material.

π-Conjugated polymer nanomaterials have been fabricated through chemical synthesis, soft/hard template based methods or self-assembled mechanism [22–24]. Among them, nanoporous

* Corresponding author.
** Corresponding author.
*** Corresponding author.
E-mail addresses: sunjong1774@kitech.re.kr (S. Lee), donghyuk@inha.ac.kr (D.H. Park), bohkim@kaist.ac.kr (B.-H. Kim).
[1] These authors contributed equally.

http://dx.doi.org/10.1016/j.orgel.2016.02.014
1566-1199/

template based synthesis has various advantages owing to its cost-effectiveness, high aspect ratio and fine controllable physical and opto-electrical properties [22]. The optical and electrical properties of nanotube- or nanowire-like structured π-conjugated polymer nanomaterials synthesized by template method have been improved [24–26]. Poly (*p*-phenylenevinylene) (PPV), which is well-known light-emitting polymer, exhibited a field emission properties when it was converted into graphitic nanotubular material embedded by gold nanoparticles [27]. However, the electrical and optical advantages of π-conjugated nanomaterials are generally lower than those of bulk during nano-engineering or carbonization procedure [27,28]. Therefore, new process or mechanism need to be developed for the simultaneous utilizing of electrical and optical multifunctional properties of π-conjugated nanomaterials.

In this work, we demonstrate enhanced and controllable multifunctional properties of poly (3-methylthiophene) (P3MT) nanotube (NT) synthesized using electrochemical template method. Photoluminescence (PL), photocurrent and field emission (FE) properties are investigated by current-voltage (*I–V*) measurement, conducting atomic force microscope (*c*-AFM), photoluminescence and photocurrent measurements are observed from P3MT NTs in the different doping states. Also, we investigate the field emission properties of P3MT NTs.

2. Materials and methods

2.1. Materials

3-methylthiophene (3-MT, 98% purified one), tetrabutylammonium hexafluorophosphate ($TBAPF_6$, 96% purified one), acetonitrile (CH_3CN), and 1-butyl-3-methylimidazolium hexafluorophosphate ($BMIMPF_6$) were purchased from Aldrich. All the chemicals were used as-received forms without further purification. Nanoporous anodic aluminum oxide (AAO) was used as a template with a pore size and height of 200 nm and 60 μm (Whatman Co.).

2.2. Synthesis and post cyclic voltammetry

The P3MT NTs were synthesized through electrochemical polymerization method on the AAO templates at −40 °C under constant current (1.4 mA at 4.5–5.0 V) as schematically shown in Fig. 1a. The electrolyte consisted of 3-MT, $TBAPF_6$, and acetonitrile as monomer, solvent and dopant, respectively. The monomer to dopant molar ratio was 5: 1 [29]. The as synthesized P3MT NTs were treated a cyclic voltammetry (CV, EC Epsilon, Bioanalytical Systems Inc.) from 0 V to 1 V with a step of 20 mV/s for 20 cycles in 0.1 M $BMIMPF_6$ at CH_3CN solution. The electrochemical window and scan rate were 0–1 V and 20 mV/s, respectively. More details of the synthetic and dedoping conditions were reported earlier [24,25,29,30].

2.3. Characterization

The structure of the P3MT NTs were measured by using scanning electron microscope (SEM; JSM-5200, JEOL) and transmission electron microscope (TEM; JEM-3010, JEOL). Optical properties, such as ultraviolet-visible (UV-Vis) absorption and PL spectrum of the P3MT NTs were investigated through UV-Vis absorption spectrometer (HP-8453), laser confocal microscope (LCM) and color charge-coupled device (CCD) experiments (see the Supporting Information for more details). The *I–V* characteristics of the isolated single strand of P3MT NTs was measured using *c*-AFM (n-Tracer, Nanofocus Inc.) with platinum/Iridium5 (PtIR5) coated tip (Nanoworld). After synthesizing P3MT NTs, AAO template was removed by hydrofluoric (HF) acid solution. The remained P3MT NTs were gathered and then homogeneously dispersed in methanol with ultrasonication for ~10 s. The dispersed P3MT NTs were drop-casted onto *p*-type doped silicon (Si) wafer and dried in a vacuum oven ($\leq 10^{-2}$ torr) for 30 min at room temperature (RT).

For the measurement of the photocurrent, P3MT NTs were deposited onto Au electrodes with a distance of 5 μm fabricated on *p*-Si/SiO_2 (~2500 Å) through a conventional photolithography method. The contact resistance between P3MT NTs and electrodes was compensated by an AC dielectrophoresis ($f = 1$ MHz, $V_{p\text{-}p} = 1$ V) [26,31]. The excitation wavelength (λ_{ex}) was 577 nm generated from a mercury-xenon lamp (Spectra-Physics 66902) combined with monochromator (Newport 77250). The *I–V* characteristics was also measured under a vacuum condition ($\leq 10^{-2}$ torr) using a Keithley 237 SMU instrument.

The field emission device (FED) was fabricated using solution drop casting method [32,33]. After drop-casting P3MT NTs dispersed in methanol on copper (Cu) anode, we measured the emission current from randomly distributed P3MT NTs under a high vacuum condition ($\leq 10^{-7}$ torr). The distance between cathode and anode was maintained at ~300 μm.

3. Result and discussion

3.1. Morphological properties of P3MT NTs

P3MT materials exhibits superior controllability as well as stability of doping level among poly (3-alkylthiophene)s due to its shortest length of alkyl side chain [34,35]. To synthesize the P3MT NTs, we used AAO (diameter ≈ 200 nm) as nanoporous template for the electrochemical synthesis with galvanostatic method (Fig. 1a). After synthesizing, post CV was treated without monomer for the control of doping level. The P3MT NTs removing template were dispersed in methanol for further experiments (see detail in Method). Fig. 1b and c are SEM images showing the side and top views of the P3MT NTs synthesized at −40 °C and then removed template. P3MT NTs have a height of about 30 μm (Fig. 1b) and an open end (Fig. 1c). From the TEM image of Fig. 1d, P3MT NTs are hollow tube-like structure with diameter and wall thickness of ~200 nm and ~10 nm, respectively.

3.2. Optical properties

Fig. 2a shows the comparison of UV-Vis absorption spectra of P3MT NTs before and after CV treatment, which were dispersed in chloroform solution. Both samples exhibit bimodal absorption characteristic peaks around ~383 nm and ~775 nm, which are corresponding to the π–π* transition and polaron/bipolaron peaks, respectively [24,29,30]. For the as-prepared P3MT NTs (hereafter referred to as P3MT NT-A), relatively broad and strong absorption around 775 nm implied a highly doped state, which was attributed to chemical doping-related electrochemical polymerization mechanism [36], and also reinforced in lower synthetic temperature [29]. However, for the P3MT NTs post-treated by CV (*i.e.*, P3MT NT-B), polaron/bipolaron peak (~775 nm) was significantly decreased indicating that the P3MT NT-B was gradually dedoped during CV process.

The change of doping state in P3MT NTs was confirmed by nanoscale LCM PL spectra (Fig. 2b). From the Gaussian decomposition of the LCM PL spectrum (see Supporting Information), the main PL peaks of P3MT NT-B were identified to locate at 634 nm and 682 nm, which were originated from 0-0 electronic transition and 0-1 vibronic mode, respectively [37–39]. After post CV treatment, the intensities of these two peaks are increased up to 38 times and 79 times, respectively, and the total PL is 20 fold

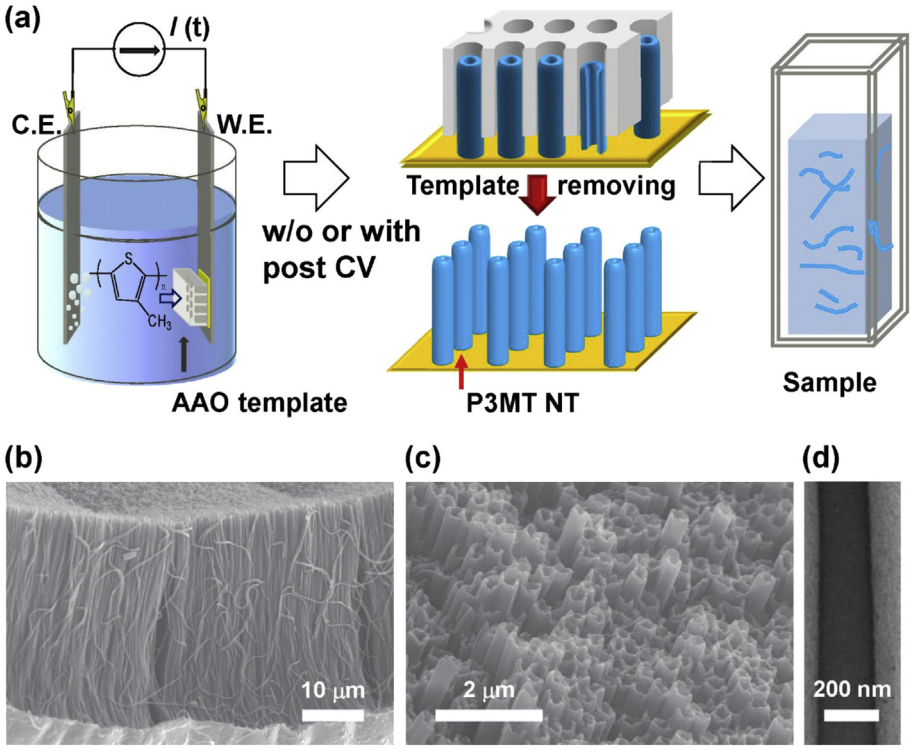

Fig. 1. (a) Schematic procedure for preparing electrochemically synthesized P3MT NTs. (b) Side-view and (c) top-view of SEM images of P3MT NTs. (d) TEM image of a single strand of P3MT NT.

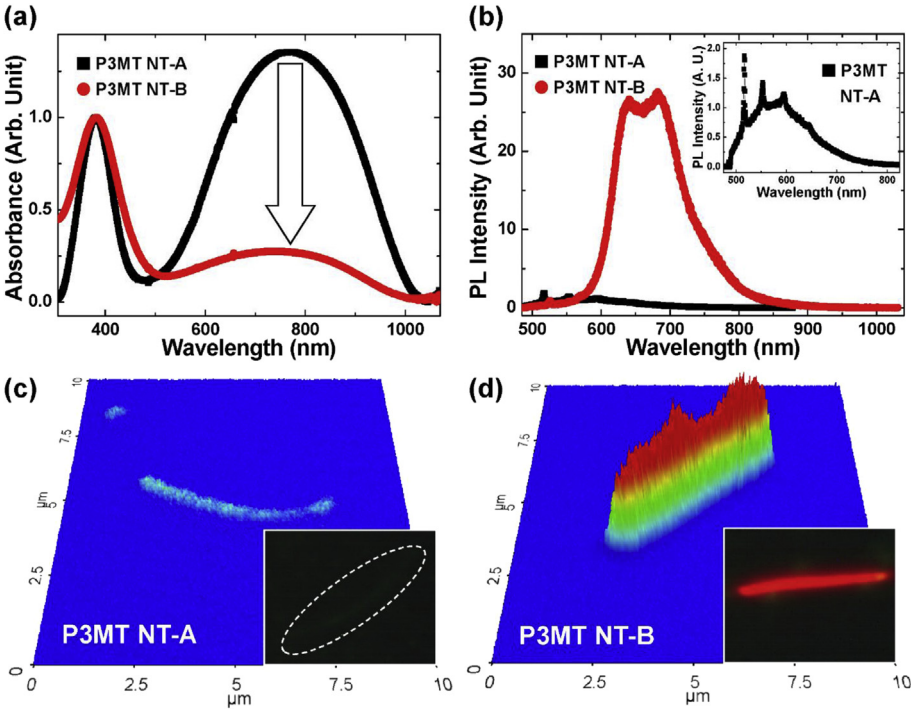

Fig. 2. (a) Comparison of UV–Vis absorption spectra of P3MT NTs before (P3MT NT-A) and after (P3MT NT-B) post CV treatment. Each spectrum was normalized with respect to the $\pi-\pi^*$ transition peak (~383 nm). (b) Comparison of normalized LCM PL spectra of the isolate single strand of the P3MT NT-A and NT-B. Inset: A magnified LCM PL spectrum of the P3MT NT-A as a reference spectrum for normalization expluding Raman mode (see Supporting Information). 3D LCM PL images of (c) P3MT NT-A and (d) P3MT NT-B. Insets: Luminescent Color CCD images of the corresponding P3MT NTs. (For interpretation of the references to color in this figure legend, the reader is referred to the web version of this article.)

enhanced compared to that of the highly doped P3MT NT-A. This clearly demonstrates the correlation between the PL intensity and

the number of polaron/bipolaron state. It is known that the high density of polaron/bipolaron state acts as PL quencher through providing a trap for excitons [40,41]. While illumination, the photoexcited polarons could be generated on the isolated polymer chains. This may significantly increase the number of bipolaron on P3MT NT-A which leads nonradiative recombination. On the while, as the number of polaron on the P3MT NT-B is relatively small, the photoexcited polaron could be singlet exciton contributing radiative decay. The main PL peak of P3MT NT-A was shown at around 587 nm, which is blue shifted compared with that shown in P3MT NT-B. This might be due to the observation of radiative decay at the undoped thiophene ring chains [42]. The variation of PL properties depending on doping level was visualized by 3-dimensional (3D) LCM PL images of a single strand of P3MT NT-A and B (Fig. 2c and d). In Fig. 2c, the PL intensity was almost quenched in 3D LCM PL image that cannot figure out where the P3MT NT-A is located from luminescent color CCD image (Inset of Fig. 2c). On the while, due to the high PL intensity it can be easily recognized a single strand of P3MT NT-B from 3D LCM PL and color CCD images (Fig. 2d and its inset). Moreover, PL was homogeneously observed from one end to the other end in a single strand of P3MT NT-B, suggesting that the doping level was well controlled in the whole P3MT NTs.

3.3. Electrical and optoelectrical properties

Electrical properties of P3MT NTs were investigated by I–V characteristic curves measured from an isolated single strand by using c-AFM (Fig. 3a). The P3MT NT-A showed ohmic behavior with a resistance of ca. 51.9 MΩ. On the while, the P3MT NT-B showed non-ohmic behavior with low current level. This is correspondence in the above optical analysis that P3MT NT-A is in the higher doping state than P3MT NT-B. Fig. 3b shows the photo-induced I–V curves of the P3MT NT-B with and without illumination (λ_{ex} = 577 nm). While the dark current of P3MT NT-B was about 0.036 mA at 3 V, the current level under illumination increased up to ca. 0.126 mA, three times larger than the dark current. This suggests that P3MT NT-B has a potential applicable for photo-detecting or photo-switching devices.

3.4. Field emission properties

Fig. 4a shows a schematic illustration of field emission device, where the cathode substrate was Cu and the anode was Au coated indium tin oxide glass substrate. P3MT NTs were drop-casted and the measurement was conducted under a pressure less than 1×10^{-7} torr. Fig. 4b shows the FE images of P3MT NTs obtained from the phosphor screen as a function of the electric field. While the light emitting spot of P3MT NT-A (upper lane) was observed from 3.5 V/μm and then continuously increases as the electric field increases, P3MT NT-B device (lower lane) showed the emitting spot from 4.5 V/μm and the screen was not fully brightened even up to the field of 6 V/μm (See Fig. S1 in Supporting Information). Fig. 4c presents the field emission characteristic curves of P3MT NTs. At the turn-on field (3.2 V/μm), the current of P3MT NT-A was drastically increased up to ca. 5×10^{-2} mA/cm^2 at 4 V/μm, which is three orders higher than that (ca. 3.5×10^{-5} mA/cm^2 at 4 V/μm) of P3MT NT-B. The maximum current density was ca. 1 mA/cm^2 at 6.5 V/μm for P3MT NT-A, two orders higher than 0.014 mA/cm^2 at 6.4 V/μm for P3MT NT-B. Moreover, the emission property of P3MT NT-A was much stable in the high electric field compared to that of P3MT NT-B. This corresponds to the expectation by a relative lower current level of P3MT NT-B in I–V characteristic curves (Fig. 3a). The inset of Fig. 4c shows a Fowler-Nordheim (FN) plot of P3MT NTs devices. The tunneling current $I = A \times F^2 \exp(-B\phi^{3/2}/F)$, where I is FE current, $F = \beta V/d = \beta E$ is local field and β is field enhancement factor, A is proportional constant, B is 6.83×10^9 V/eV$^{3/2}$m and ϕ is work function of material, respectively [27,43]. In this experiment, we used the HOMO level (−4.99 eV) of P3MT instead of work function [44–46]. From the fitting slopes in the inset of Fig. 4c plotted $\ln(I/E^2)$ versus $1/E$, the β_1 was ca. 8270 for P3MT NT-A and ca. 889 for P3MT NT-B, which is almost comparable to the value of CNT [47,48]. This result, although P3MT NTs have much structural defects and a high density of nanotubes, might come from the high aspect ratio and lower work function of highly doped P3MT NT-A [49,50]. To test the stability of FE device using P3MT NT-A, the emission current was measured at 6 V/μm for 30 min. As shown in Fig. 4d, the emission current was rather stable without device failure during the test. However, the current density gradually decreased to about 90% of the initial current level after 30 min, which is caused by the weak thermal durability of polymer tip even though low work function and high β value. As a result, this FE properties of P3MT NTs provides a potential probability for the application of field emission devices.

4. Conclusion

Up to now, we have demonstrated the multifunctional properties of P3MT NTs. Using the nanoporous template and electrochemical polymerization method, the structural property of P3MT NTs was engineered. Through the post CV process, we controlled

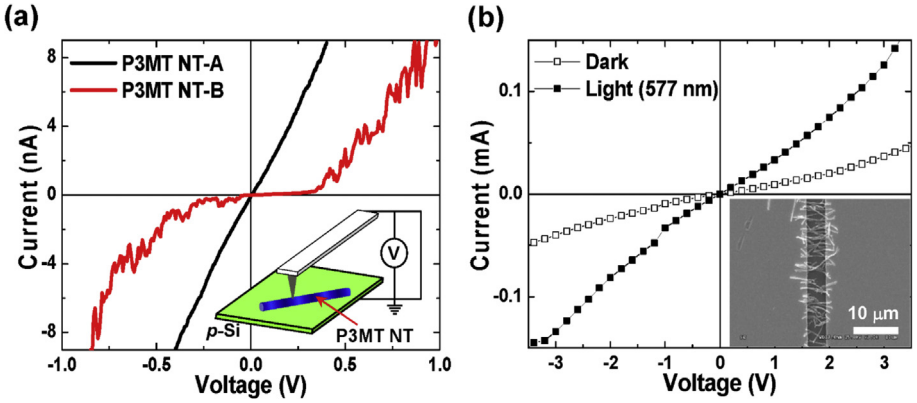

Fig. 3. (a) I–V characteristic curves of the isolated single strand of the pristine (NT-A) and dedoped (NT-B) P3MT NT by using c–AFM. Inset: Schematic illustration of measurement setup. (b) A comparison of the I–V characteristic curves of the P3MT NTs-B under the dark and photo-excited conditions. Inset: SEM image of the P3MT NTs-B onto the bottom-contacted 2-probe electrodes.

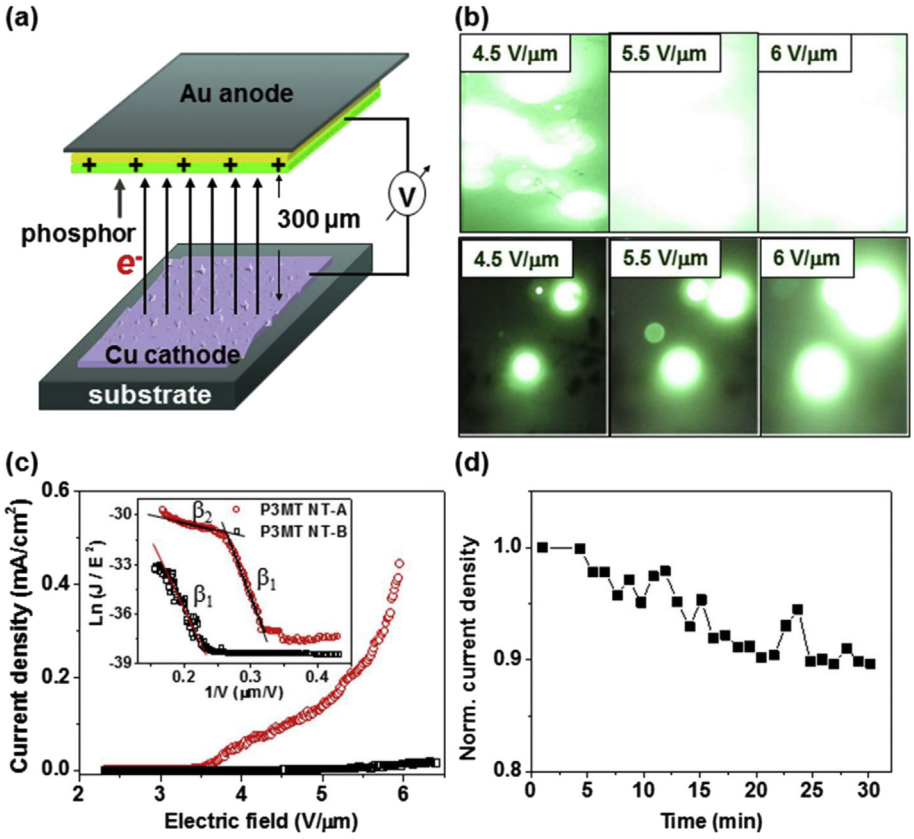

Fig. 4. (a) Schematic diagram of the FE cell. (b) A comparison of FE images of the P3MT NTs-A [top] and P3MT NTs-B [bottom] through green phosphor screen. (c) $J-E$ characteristic curves of the P3MT NTs-A (□) and NTs-B (○). Inset: FN Plot of Fig. 4c. (d) Time dependent ($J-t$) FE characteristics of the P3MT NTs-A. (For interpretation of the references to color in this figure legend, the reader is referred to the web version of this article.)

the doping level of P3MT NTs, which induced the variation of $I-V$ characteristics, photocurrent, and field emission property of P3MT NTs. This result shows that the multifunctional properties of nanostructured π-conjugated polymers can be simultaneously controlled for the applications of multifunctional organic nanodevices.

Author contributions

Y. K. Hong, S. Kim, and H. T. Kim carried out the most experiments, S. Lee, and B. G. Kim provided experimental supports, Y. K. Hong, S. Lee, D. H. Park, and B. H. Kim conceived, designed the experiments, and analyzed the results. All the authors wrote and reviewed the manuscript.

Competing interest

The authors declare no competing financial interest.

Acknowledgements

This research was supported by the KUSTAR-KAIST Institute, Korea, under the R&D program (N01150490) supervised by KAIST. This research was also supported in part by the National Research Foundation of Korea (NRF) grant funded by the Ministry of Education, Science and Technology (NRF-2013R1A1A1012445) and Hwaam foundation. Support by the Inha University Research Grant (Grant No. INHA-49290) is gratefully acknowledged.

Appendix A. Supplementary data

Supplementary data related to this article can be found at http://dx.doi.org/10.1016/j.orgel.2016.02.014.

References

[1] E. Roduner, Size matters: why nanomaterials are different, Chem. Soc. Rev. 35 (2006) 583–592.
[2] A.D. Yoffe, Low-dimensional systems: quantum size effects and electronic properties of semiconductor microcrystallites (zero-dimensional systems) and some quasi-two-dimensional systems, Adv. Phys. 42 (1993) 173–262.
[3] K. Roy, M. Padmanabhan, S. Goswami, T.P. Sai, G. Ramalingam, S. Raghavan, A. Ghosh, Graphene-MoS_2 hybrid structures for multifunctional photoresponsive memory devices, Nat. Nanotechnol. 8 (2013) 826–830.
[4] P. Xu, X. Han, B. Zhang, Y. Du, H.L. Wang, Multifunctional polymer-metal nanocomposites via direct chemical reduction by conjugated polymers, Chem. Soc. Rev. 43 (2014) 1349–1360.
[5] L. Feng, C. Zhu, H. Yuan, L. Liu, F. Lv, S. Wang, Conjugated polymer nanoparticles: preparation, properties, functionalization and biological applications, Chem. Soc. Rev. 42 (2013) 6620–6633.
[6] J.A. Misewich, R. Martel, P. Avouris, J.C. Tsang, S. Heinze, J. Tersoff, Electrically induced optical emission from a carbon nanotube FET, Science 300 (2003) 783–786.
[7] M. Freitag, J. Chen, J. Tersoff, J.C. Tsang, Q. Fu, J. Liu, P. Avouris, Mobile ambipolar domain in carbon-nanotube infrared emitters, Phys. Rev. Lett. 93 (2004) 0768031–0768034.
[8] J.H. He, T.H. Wu, C.L. Hsin, K.M. Li, L.J. Chen, Y.L. Chueh, L.J. Chou, Z.L. Wang, Beaklike SnO_2 nanorods with strong photoluminescent and field-emission properties, Small 2 (2006) 116–120.
[9] R.H. Friend, R.W. Gymer, A.B. Holmes, J.H. Burroughes, R.N. Marks, C. Taliani, D.D.C. Bradley, D.A. Dos Santos, J.L. Brédas, M. Lögdlund, W.R. Salaneck, Electroluminescence in conjugated polymers, Nature 397 (1999) 121–128.
[10] A.J. Heeger, N.S. Sariciftci, E.B. Namdas, Semiconducting and Metallic Polymers, Oxford University Press, Oxford, 2010.
[11] X. Huang, P. Sheng, Z. Tu, F. Zhang, J. Wang, H. Geng, Y. Zou, C.A. Di, Y. Yi, Y. Sun, W. Xu, D. Zhu, A two-dimensional π-d conjugated coordination

polymer with extremely high electrical conductivity and ambipolar transport behaviour, Nat. Commun. 6 (2015) 7408.
[12] K.J. Van Schooten, D.L. Baird, M.E. Limes, J.M. Lupton, C. Boehme, Probing long-range carrier-pair spin-spin interactions in a conjugated polymer by detuning of electrically detected spin beating, Nat. Commun. 6 (2015) 6688.
[13] A. Kros, S.W.F.M. Van Hövell, N.A.J.M. Sommerdijk, R.J.M. Nolte, Poly(3,4-ethylenedioxythiophene)-based glucose biosensors, Adv. Mater. 13 (2001) 1555–1557.
[14] Y. Xia, P. Yang, Y. Sun, Y. Wu, B. Mayers, B. Gates, Y. Yin, F. Kim, H. Yan, One-dimensional nanostructures: synthesis, characterization, and applications, Adv. Mater. 15 (2003) 353–389.
[15] H. Liu, C.H. Reccius, H.G. Craighead, Single electrospun regioregular poly(3-hexylthiophene) nanofiber field-effect transistor, Appl. Phys. Lett. 87 (2005) 253106.
[16] S.I. Cho, W.J. Kwon, S.J. Choi, P. Kim, S.A. Park, J. Kim, S.J. Son, R. Xiao, S.H. Kim, S.B. Lee, Nanotube-based ultrafast electrochromic display, Adv. Mater. 17 (2005) 171–175.
[17] G.A. O'Brien, A.J. Quinn, D.A. Tanner, G. Redmond, A single polymer nanowire photodetector, Adv. Mater. 18 (2006) 2379–2383.
[18] S. Berson, R. De Bettignies, S. Bailly, S. Guillerez, Poly(3-hexylthiophene) fibers for photovoltaic applications, Adv. Funct. Mater. 17 (2007) 1377–1384.
[19] M. Muccini, A bright future for organic field-effect transistors, Nat. Mater. 5 (2006) 605–613.
[20] J. Zaumseil, R.H. Friend, H. Sirringhaus, Spatial control of the recombination zone in an ambipolar light-emitting organic transistor, Nat. Mater. 5 (2006) 69–74.
[21] K. Muhieddine, M. Ullah, B.N. Pal, P. Burn, E.B. Namdas, All solution-processed, hybrid light emitting field-effect transistors, Adv. Mater. 26 (2014) 6410–6415.
[22] C.R. Martin, Nanomaterials: a membrane-based synthetic approach, Science 266 (1994) 1961–1966.
[23] A. Huczko, Template-based synthesis of nanomaterials, Appl. Phys. A Mater. Sci. Process. 70 (2000) 365–376.
[24] Y.K. Hong, D.H. Park, S.H. Lee, J. Joo, Synthesis, characteristics, and applications of intrinsically light-emitting polymer nanostructures, Adv. Polym. Sci. 259 (2013) 201–244.
[25] D.H. Park, M.S. Kim, J. Joo, Hybrid nanostructures using π-conjugated polymers and nanoscale metals: synthesis, characteristics, and optoelectronic applications, Chem. Soc. Rev. 39 (2010) 2439–2452.
[26] Y.K. Hong, D.H. Park, S.G. Jo, M.H. Koo, D.C. Kim, J. Kim, J.S. Kim, S.Y. Jang, J. Joo, Fine characteristics tailoring of organic and inorganic nanowires using focused electron-beam irradiation, Angew. Chem. Int. Ed. 50 (2011) 3734–3738.
[27] K. Kim, S.H. Lee, W. Yi, J. Kim, J.W. Choi, Y. Park, J.I. Jin, Efficient field emission from highly aligned, graphitic nanotubes embedded with gold nanoparticles, Adv. Mater. 15 (2003) 1618–1622.
[28] K. Kim, J.I. Jin, Preparation of PPV nanotubes and nanorods and carbonized products derived therefrom, Nano Lett. 1 (2001) 631–636.
[29] D.H. Park, B.H. Kim, M.G. Jang, K.Y. Bae, J. Joo, Characteristics and photoluminescence of nanotubes and nanowires of poly (3-methylthiophene), Appl. Phys. Lett. 86 (2005) 113116.
[30] D.H. Park, H.S. Kim, M.Y. Jeong, Y.B. Lee, H.J. Kim, D.C. Kim, J. Kim, J. Joo, Significantly enhanced photoluminescence of doped polymer-metal hybrid nanotubes, Adv. Funct. Mater. 18 (2008) 2526–2534.
[31] R. Krupke, F. Hennrich, H.B. Weber, M.M. Kappes, H.V. Löhneysen, Simultaneous deposition of metallic bundles of single-walled carbon nanotubes using ac-dielectrophoresis, Nano Lett. 3 (2003) 1019–1023.
[32] J. Joo, B.H. Kim, D.H. Park, H.S. Kim, D.S. Seo, J.H. Shim, S.J. Lee, K.S. Ryu, K. Kim, J.I. Jin, T.J. Lee, C.J. Lee, Fabrication and applications of conducting polymer nanotube, nanowire, nanohole, and double wall nanotube, Synth. Met. 153 (2005) 313–316.
[33] J. Joo, S.J. Lee, D.H. Park, Y.S. Kim, Y. Lee, C.J. Lee, S.R. Lee, Field emission characteristics of electrochemically synthesized nickel nanowires with oxygen plasma post-treatment, Nanotechnology 17 (2006) 3506–3511.
[34] K. Yoshino, S. Morita, M. Uchida, K. Muro, T. Kawai, Y. Ohmori, Novel electrical and optical properties of poly(3-alkylthiophene) as function of alkyl chain length and their functional applications, Synth. Met. 55 (1993) 28–35.
[35] Y. Pang, X. Li, H. Ding, G. Shi, L. Jin, Electropolymerization of high quality electrochromic poly(3-alkyl-thiophene)s via a room temperature ionic liquid, Electrochim. Acta 52 (2007) 6172–6177.
[36] S. Sadki, P. Schottland, N. Brodie, G. Sabouraud, The mechanisms of pyrrole electropolymerization, Chem. Soc. Rev. 29 (2000) 283–293.
[37] P.J. Brown, D.S. Thomas, A. Köhler, J.S. Wilson, J.S. Kim, C.M. Ramsdale, H. Sirringhaus, R.H. Friend, Effect of interchain interactions on the absorption and emission of poly(3-hexylthiophene), Phys. Rev. B 67 (2003) 642031–6420316.
[38] T. Kobayashi, J.I. Hamazaki, H. Kunugita, K. Ema, T. Endo, M. Rikukawa, K. Sanui, Coexistence of photoluminescence from two intrachain states in polythiophene films, Phys. Rev. B 67 (2003) 2052141–2052147.
[39] J. Clark, C. Silva, R.H. Friend, F.C. Spano, Role of intermolecular coupling in the photophysics of disordered organic semiconductors: aggregate emission in regioregular polythiophene, Phys. Rev. Lett. 98 (2007) 206406.
[40] J.C. Bolinger, M.C. Traub, T. Adachi, P.F. Barbara, Ultralong-range polaron-induced quenching of excitons in isolated conjugated polymers, Science 331 (2011) 565–567.
[41] P. Dyreklev, O. Inganäs, J. Paloheimo, H. Stubb, Photoluminescence quenching in a polymer thin-film field-effect luministor, J. Appl. Phys. 71 (1992) 2816–2820.
[42] S. Hayashi, K. Kaneto, K. Yoshino, Quenching of photoluminescence in poly(thiophene) films by electrochemical doping, Solid State Commun. 61 (1987) 249–251.
[43] J.M. Bonard, K.A. Dean, B.F. Coll, C. Klinke, Field emission of individual carbon nanotubes in the scanning electron microscope, Phys. Rev. Lett. 89 (2002) 1976021–1976024.
[44] Z.W. Sun, A.J. Frank, Characterization of the intrachain charge-generation mechanism of electronically conductive poly (3-methylthiophene), J. Chem. Phys. 94 (1991) 4600–4608.
[45] L.J.A. Koster, V.D. Mihailetchi, P.W.M. Blom, Ultimate efficiency of polymer/fullerene bulk heterojunction solar cells, Appl. Phys. Lett. 88 (2006) 093511.
[46] B.M. Omer, A. Khogali, A quantum chemical study on polythiophenes derivatives as donor materials in bulk-heterojunction polymer solar cell, Res. J. Appl. Sci. Eng. Technol. 4 (2012) 3768–3774.
[47] Y. Zuo, Y. Ren, Z. Wang, X. Han, L. Xi, Enhanced field emission and hysteresis characteristics of aligned carbon nanotubes with Ti decoration, Org. Electron. 14 (2013) 2306–2314.
[48] D.H. Shin, K.N. Yun, S.G. Jeon, J.I. Kim, Y. Saito, W.I. Milne, C.J. Lee, High performance field emission of carbon nanotube film emitters with a triangular shape, Carbon 89 (2015) 404–410.
[49] R. Zou, J. Hu, Y. Song, N. Wang, H. Chen, H. Chen, J. Wu, Y. Sun, Z. Chen, Carbon nanotubes as field emitter, J. Nanosci. Nanotechnol. 10 (2010) 7876–7896.
[50] M.S. Wang, J.Y. Wang, L.M. Peng, Engineering the cap structure of individual carbon nanotubes and corresponding electron field emission characteristics, Appl. Phys. Lett. 88 (2006) 243108.